Indian Journal of Pure & Applied Physics
Vol. 62, April 2024, pp. 292-303
DOI: 10.56042/ijpap.v62i4.7435

Comparative Study of Lead-free Perovskite Materials $MASnI_3$, $MASnBr_3$ and $MAGeI_3$ to Design, Simulate and Optimize Lead Free PSC

Nishi Bala[a,b*] & Sanjeev Kumar Mallik[a]

[a]Department of Electrical Engineering, National Institute of Technology, Patna 800 005, Bihar, India

[b]Department of Electrical and Electronics Engineering, Bakhtiyarpur College of Engineering, Champapur, Dedaur, Bakhtiyarpur 803 212, Bihar, India

Received 19 December 2023; accepted 22 January 2024

The advancement of photovoltaic technology has certainly been revamped by lead-based perovskite solar cells (PSCs). But lead toxicity is a big hurdle in its large-scale commercial production and usage. Hence, in current work three lead-free Perovskite materials $MASnI_3$, $MASnBr_3$ and $MAGeI_3$ has been thoroughly investigated to develop environment friendly PSCs of high efficiency and stability. The modelled device structures utilized ZnO as electron transport layer (ETL), $CH_3NH_3SnI_3$, $CH_3NH_3SnBr_3$ and $CH_3NH_3GeI_3$ as perovskite absorption layer (PAL), Spiro-OMeTAD as hole transport layer (HTL), Indium doped tin oxide (ITO) as top electrode and Au as anode contact. Defect density in combination with different thickness of perovskite absorption layer has been investigated to obtain optimum solar cell parameters. At a thickness of 500 nm and defect density of $1 \times 10^{14} cm^{-3}$ of PAL, simulated Perovskite solar cell ITO/ZnO/$CH_3NH_3SnI_3$/Spiro-OMeTAD/Au provided optimized solar cell parameters as PCE 25.95%, Voc 1.06V, Jsc 31.67mA/cm^2 and FF 77.24%, ITO/ZnO/$CH_3NH_3SnBr_3$/Spiro-OMeTAD/Au provided PCE 25.01%, V_{OC} 1.02V, J_{SC} $32.41 mA/cm^2$ and FF 75.68%, ITO/ZnO/$CH_3NH_3SnI_3$/Spiro-OMeTAD/Au provided PCE 19.66%, V_{OC} 1.81V, J_{SC} $14.29 mA/cm^2$ and FF 75.95%. Further, effect of interface defect density, series resistance, shunt resistance, and temperature are studied on the solar cell characteristics. It is well observed that Sn-based devices are more efficient and less stable than Ge-based devices and vice versa.

Keywords: ETL-Electron transport layer; PSC–Perovskite solar cell; PAL – Perovskite absorption layer; PCE – Power conversion efficiency

1 Introduction

The majority of the world's energy needs are currently fulfilled by the fossil fuel. However, as energy consumption rises, fossil fuel reserves are being depleted quickly. Alternative to this are renewable energy sources which must be developed to meet expanding demand for energy. Sunlight-powered energy is one of the most promising developments in meeting the growing global energy demands among the various sustainable sources[1-2].

Perovskites Solar cells having structure ABX3 (Here A is organic/inorganic cation, B is Pb/Sn cation, and X is halide anion) has revolutionized the development of photovoltaic technology. The PCE of lead-based PSCs has increased rapidly over past few years, rising from 3.9% to a certified 25.8%[3-7]. The exceptional optoelectronic characteristics like the high absorption capacity, less carrier binding energy and long diffusion length are attributed for the remarkable increase in PCE[8-9]. Currently, high PCE is achieved by lead-based perovskite solar cells. However, toxicity of Pb raises worries about environmental contamination and health issues, which severely restricts both its large-scale manufacturing and its commercial usage[10]. In order to create the PSCs of the future generation, environment friendly lead-free perovskite materials are widely sought.

There have been several lead-free perovskite materials investigated so far, but Tin (Sn), and Germanium (Ge), based perovskite standout as the most viable contender. Sn perovskites display a matching band gap around the Shockley-Queisser limit (1.3-1.4 eV). Sn and Pb have similar outer cell configurations (ns2 np2), also having same atomic size[11]. The methyl ammonium tin iodide ($MASnI_3$) and methyl ammonium tin bromide ($MASnBr_3$), have direct bandgaps of around 1.20 and 1.30[12] respectively. The $MASnI_3$ perovskite, which has a band gap (Eg) of 1.3 eV, was employed in solar cells and generated a PCE of 6.4%. The +2-oxidation state of Sn, required for the development of a perovskite becomes unstable upon exposure to oxygen or air

*Corresponding author: (E-mail: nishib.phd19.ee@nitp.ac.in)

humidity and rapidly oxidizes to the +4 state[13-17]. This has an impact on the operating environment of the device and the manufacturing process for Sn-based solar cells. Researchers discovered that adjusting the halide ions in the perovskite structure may increase the device stability. In this regard, several more efforts to construct effective low band gap PSCs based on Sn have been undertaken[18-20].

Ge, an element in group 14 along with Sn and Pb, is yet another alternative to lead that may be used for PSCs because it is more covalent and has a greater electro negativity than lead[21]. Due to its mercurial nature in +2 oxidation state, germanium halide perovskites have been explored experimentally only sometimes, despite the fact that several theoretical studies have shown their potential for solar cell applications[22-23]. Due to the characteristics of Ge, like narrow bandgap (>1.6 eV), a lower ionic radius, and poor solubility in polar solvents, the PCE of Ge-based PSC is still around 5%[24-26]. But Germanium (Ge) may be utilized in perovskite material because it is more stable and environment friendly. Additionally, Germanium (Ge) is less prone to degradation than Lead (Pb), so it can be more stable with the active layer of $MAGeI_3$ than $MAPbI_3$, and its improved stability at high temperatures up to 150 °C makes it suitable for the production of PSC devices[27]. Accordingly, both Tin and Germanium based Perovskite material having distinct property may be utilized in development of lead-free PSCs with optimum characteristics. Device performance is significantly impacted by CTMs (*i.e.*, HTMs and ETMs), which decide how carriers are separated and transported in PSCs[28]. An increasingly significant challenge is the fabrication of carrier transport materials/layers (CTLs) based on various device architectures. For effective and stable PSCs, stable CTLs with superior electrical characteristics and appropriate energy levels are required[29]. ZnO is selected as ETL material because it is inexpensive, has a suitable work function, stability, excellent light transmittance, superior electron mobility and environmental friendliness[30]. For HTL, Spiro-OMeTAD is taken because ionization potential of Spiro-OMeTAD matches well with the light harvesting layer and best glass-forming properties of Spiro-OMeTAD provides good contact at their interfaces[31].

The objective of the current work is to investigate Sn and Ge-based perovskite material to develop environment friendly lead-free PSCs. Comprehensive study of three perovskite material $CH_3NH_3SnI_3$, $CH_3NH_3SnBr_3$ and $CH_3NH_3GeI_3$ has been accomplished for the modelling of lead-free PSCs. Effect of factors like thickness, defect density of PAL, interface defect density, series and shunt resistance of device and temperature on the performance of PSC structures ITO/ZnO/$CH_3NH_3SnI_3$/Spiro-OMeTAD/Au, ITO/ZnO/$CH_3NH_3SnBr_3$/Spiro-OMeTAD/Au and ITO/ZnO/$CH_3NH_3GeI_3$/Spiro-OMeTAD/Au has been thoroughly investigated for the optimum results. Standard deep energy defect level of 0.6 eV is considered for the current study. For the modelled PSC structures, basic characteristics such as V_{OC}, J_{SC}, PCE and FF were examined. The device modelling and illustration of result of different parameter requires software simulation and numerical modelling. Solar cell capacitance simulator (SCAPS) application is used for this purpose[32]. The PSC device structures are illuminated by the AM 1.5 solar spectrum.

This paper contains five sections. In section 1 introduction of PSC devices its growth story and limitations, reason to choose lead-free PSC devices and also its limitations have been discussed. In the section 2, PSC device structures has been discussed, its schematic diagram, energy band diagram and the carrier transport mechanism inside device has been explained. section 3 deals with theoretical modelling and equations involved in simulations. In the section 4, various results of solar cell parameter that are obtained by varying defect densities, width of PAL, interface defect densities, series resistances, shunt resistances and temperature has been discussed. Comparison of solar cell parameter of all three PSC devices have been studied. Optimum result of PCE that is obtained on a specific design parameter has been discussed and its comparison with previous works has been done. In the section 5, conclusion has been provided and future works are recommended for further enhancement of PCE and other solar cell parameters.

2 Device architecture and modelling

Three different lead-free PSCs, two from Sn family and one from Ge family having a configuration of ITO/ZnO/$CH_3NH_3SnI_3$/Spiro-OMeTAD/Au,ITO/ZnO/$CH_3NH_3SnBr_3$/Spiro-OMeTAD/Au and ITO/ZnO/$CH_3NH_3GeI_3$/Spiro-OMeTAD/Au have been modelled with same ETL, HTL, anode and cathode. The proposed PSC devices as shown in Fig. 1(a) are modelled using ITO, which works as a top electrode

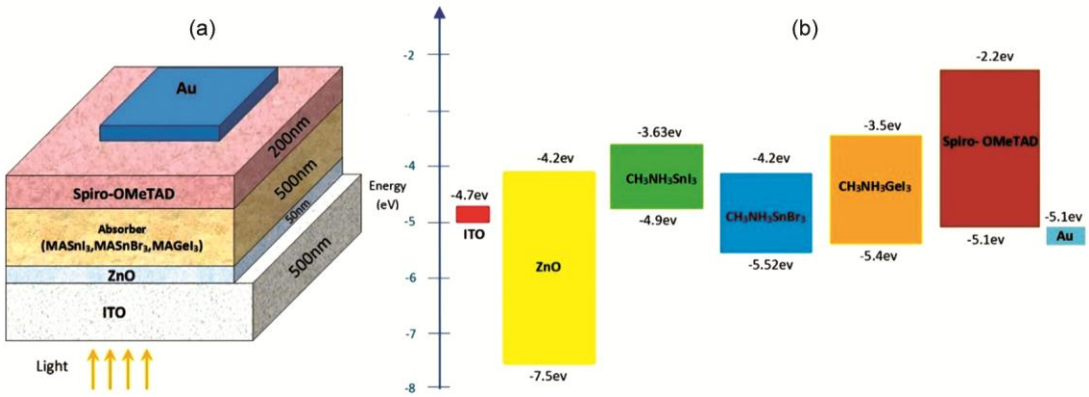

Fig. 1 — (a) Schematic diagram of proposed PSC device (b) Energy band diagram and the carrier transport mechanism in $CH_3NH_3SnI_3$, $CH_3NH_3SnBr_3$and $CH_3NH_3GeI_3$ based PSC devices.

is of 500 nm thickness, ZnO as an ETL of width 50 nm, Spiro-OMeTAD as a HTL of width 200 nm. Width of PAL has been varied for obtaining optimum solar cell parameters, which was found 500nm for all the devices. Hence, width of PAL is taken 500nm. Au works as the anode. Fig. 1(b) represents the working mechanism in the device. It shows band diagram with respect to vacuum level. The PAL absorbs solar spectrum photons whose energy is more than its bandgap and generate electron and hole pairs in the conduction and valance band respectively. Energy bands i.e. conduction band and valence band of sandwiched layers are compatible such that it allows smooth transport of carriers. Electron and hole pairs are generated in perovskite absorption layer. Electron moves in conduction band of PAL to ETL which is further collected at ITO. Hole moves in valence band of PAL to HTL and further collected at electrode Au. The ETL and HTL are well known for their critical roles in perovskite solar cells. They effectively move the generated charge carriers from the absorber to the appropriate contacts while simultaneously obstructing electron and hole movement towards non desired contacts. This prevents charge recombination at the interfaces between the absorber/HTL and the ETL/absorber. At the ETL/absorber and absorber/ HTL interfaces, the conduction and valence band offsets (CBO and VBO) have a major impact on the charge separation and directly control device performance. CBO and VBO is defined as follow:

$$CBO = \chi_{Absorber} - \chi_{ETL}$$
$$VBO = \chi_{HTL} + E_{g\,(HTL)} - (\chi_{Absorber} + E_{g\,(Absorber)})$$

Where χ is electron affinity and Eg is band gap of corresponding layers. Numerous research reveals that for smooth conduction and superior solar cell parameters CBO and VBO must be in the range of -0.3ev to +0.3ev.

ZnO as ETL and Spiro-OMeTAD as HTL fulfills criterion of CBO and VBO. CBO and VBO for all three devices are calculated by taking the data from Table 1.

For ITO/ZnO/$CH_3NH_3SnI_3$/Spiro-OMeTAD/Au, CBO = 0.2eV, V.B.O = 0.12eV,
for ITO/ZnO/ $CH_3NH_3SnBr_3$/Spiro-OMeTAD/Au, CBO = 0.17ev, VBO = 0.15ev and
for ITO/ZnO/ $CH_3NH_3GeI_3$/Spiro-OMeTAD/Au, CBO = -0.02ev, VBO = -0.26.

3 Theoretical modelling and equations

The SCAPS-1D primarily used numerical modelling based on four set of electronic device equations as follows:

1 Poisson's equation

$$-\frac{d^2\emptyset(x)}{dx^2} = \frac{dE}{dx} = \frac{\rho}{\epsilon} = \frac{q(p-n+N_D^+-N_A^-\pm N_{def})}{\epsilon_0\epsilon_r}$$

Where $\emptyset$ is electric potential, E is strength of electric field, ρ is charge density, ϵ is permittivity, q is fundamental unit of charge, n and p are the concentration of electron and hole respectively. N_D^+ and N_A^- are concentration of donor and acceptor ions. N_{def} is concentration of defect density of donor and acceptor.

2 Continuity equation

$$-\frac{1}{q}\left(\frac{dJ_e}{dx}\right) = G - R$$
$$\frac{1}{q}\left(\frac{dJ_n}{dx}\right) = G - R$$

Where, $\frac{dJ_e}{dx}$ is variation of electron current density with position, $\frac{dJ_n}{dx}$ is variation of hole current density

with position,G is carrier generation rate and R is carrier recombination rate.

3 Current density equation

$$J_e = q\left(n\mu_e E + D_e \frac{dn}{dx}\right)$$

$$J_n = q\left(n\mu_n - D_n \frac{dp}{dx}\right)$$

Where, J_e, J_n are electron and hole current density respectively. μ_e, μ_n are electron and hole mobility respectively. D_e, D_n are diffusion current constant.

4 Results and discussion

Comprehensive analysis of all proposed devices has been done in order to obtain optimized result for electrical solar cell parameters *i.e.* V_{OC}, J_{SC}, FF and PCE. The effect of thickness and defect density of the PAL on the PSC devices have been investigated to obtain specific PSC device which provide maximum PCE. Furthermore, impact of interface defect density of ETL/ Perovskite and HTL/ Perovskite layers on the PCE has been obtained and discussed. Standard deep energy defect level of 0.6eV is considered. Effect of variation of defect density on the diffusion length and lifetime of carrier has also been obtained. Contour of V_{OC}, J_{SC}, FF and PCE as a joint function of defect density and PAL thickness is drawn and obtained optimized result has been discussed. Comparative quantum efficiency of all PSCs has been studied which specifically relate number of charge carriers generated on different wavelength of sun spectrum. J-V characteristics of all three absorber PSCs has been plotted and shown in Fig. 2(a). In Fig. 2(b) relation of

Table 1 — The properties of materials and simulation parameters in $CH_3NH_3SnI_3$, $CH_3NH_3SnBr_3$ and $CH_3NH_3GeI_3$based PSC device[33-37].

Parameters	ITO	ZnO	$CH_3NH_3SnI_3$	$CH_3NH_3SnBr_3$	$CH_3NH_3GeI_3$	Spiro-OMeTAD
Thickness (nm)	500	50	500	500	500	200
E_g(eV)	3.5	3.3	1.3	1.3	1.9	3.17
Electron Affinity (eV)	4	4	4.2	4.17	3.98	2.45
Relative permittivity	9	9	10	10	10	3
Conduction band effective density of states$N_c(cm^{-3})$	2.2×10^{18}	2.2×10^{18}	1×10^{18}	2.2×10^{18}	1×10^{16}	2.2×10^{18}
Valence band effective density of states$N_v(cm^{-3})$	1.8×10^{19}	1.8×10^{19}	1×10^{18}	1.8×10^{18}	1×10^{15}	1.9×10^{19}
Thermal velocity of electron (cm/s)	1×10^{7}	1×10^{7}	1×10^{7}	1×10^{7}	1×10^{7}	1×10^{7}
Thermal velocity of hole (cm/s)	1×10^{7}	1×10^{7}	1×10^{7}	1×10^{7}	1×10^{7}	1×10^{7}
Mobility of electron μ_e (cm^2/Vs)	20	100	1.6	1.6	16.2	2×10^{-4}
Mobility of hole μ_h (cm^2/Vs)	10	25	1.6	1.6	10.1	2×10^{-4}
Donor density $N_D(cm^{-2})$	1×10^{21}	1×10^{18}	0	1×10^{13}	1×10^{9}	0
Acceptor density $N_A(cm^{-2})$	0	0	3.2×10^{15}	1×10^{13}	1×10^{9}	1×10^{18}
$N_t(cm^{-3})$	1×10^{15}	1×10^{15}	1×10^{14}	1×10^{14}	1×10^{14}	1×10^{14}

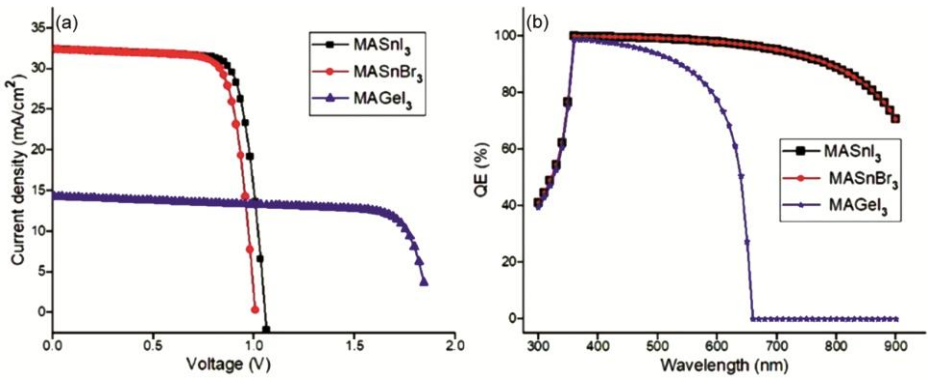

Fig. 2 — (a) J-V graph of proposed PSC devices (b) Variation of QE with wavelength of the proposed PSC device.

QE and wavelength of the proposed PSC devices is shown. QE increases with wavelength and found maximum at nearly 370nm for all three-absorber material. Then after 370nm,value of QE for $CH_3NH_3GeI_3$ is decreased more rapidly than $CH_3NH_3SnI_3$ and $CH_3NH_3SnBr_3$. After 670nm wavelength QE of Ge absorber becomes zero. This happened due to different band gap of absorber materials.

4.1 Effect of PAL thickness variations on PSC parameters

Effect of variation of PAL thickness at the practically achievable defect density of $1\times10^{14}cm^{-3}$ is analyzed for all devices. Comparative result of V_{OC}, J_{SC}, FF and PCE is obtained for thickness variation of PAL from 200nm to 900nm and shown in Fig. 3(a)-(d). V_{OC} is slightly decreased for $CH_3NH_3SnI_3$ and $CH_3NH_3SnBr_3$ with the increase in PAL thickness while V_{OC} of $CH_3NH_3GeI_3$ is nearly constant for increasing width from 200nm to 900nm. J_{SC} for all three PAL materials increased continuously with increase in PAL thickness. But after 500nm thickness, value of J_{SC} increased slowly and further move towards saturation. This happen because increase in PAL thickness allow absorption of more solar photon, which generate more charge carrier pairs and consequently higher current density. But further increase in width causes increased rate of recombination of charge carriers, hence J_{SC} reach toward saturation at 900nm. FF is reduced sharply and linearly for $CH_3NH_3SnBr_3$ and $CH_3NH_3GeI_3$ and with increase of width from 200nm to 900nm, for $CH_3NH_3SnI_3$ FF decrease up to 400nm width then after it become nearly constant with increase in width. The PCE is increased linearly with increase in PAL width from 200nm to 500nm for all PSCs, due to increased current density after 500 nm, PCE becomes almost constant with further increase in width due to increased rate of recombination. From width variation analysis it is observed that 500nm width of PAL is suitable for design of all the three materials PSCs. Table 2 shows performance parameters of all three proposed devices at 500nm of width of PAL.

Table 2 — Performance of the Simulated devices.

Optimized PSC	V_{OC}(V)	J_{SC}(mA/cm^2)	FF (%)	PCE (%)
ITO/ZnO/$CH_3NH_3SnI_3$/Spiro-OMeTAD/Au	1.06	31.67	77.24	25.95
ITO/ZnO/$CH_3NH_3SnBr_3$/Spiro-OMeTAD/Au	1.02	32.41	75.68	25.01
ITO/ZnO/$CH_3NH_3GeI_3$/Spiro-OMeTAD/Au	1.81	14.29	75.95	19.66

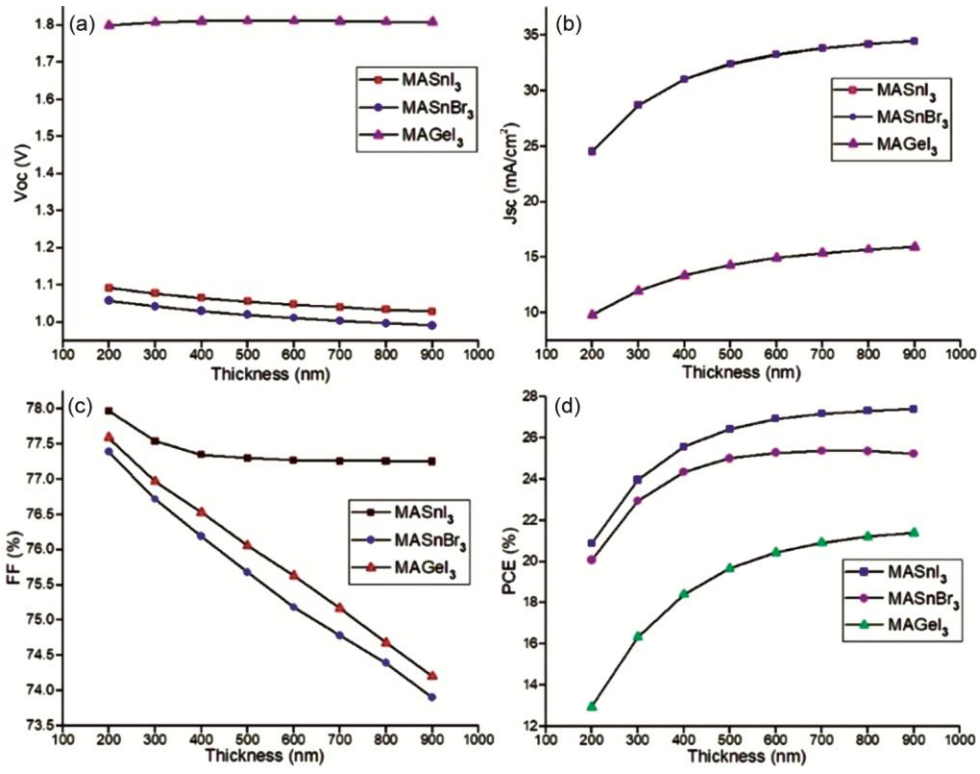

Fig. 3 — Characteristics of (a) V_{OC}(b) J_{SC} (c) FF and (d) PCE with the thickness of $CH_3NH_3SnI_3$, $CH_3NH_3SnBr_3$ and $CH_3NH_3GeI_3$.

The optimum result is achieved by varying the several parameters like PAL width, defect density, interface defect density between ETL/PAL and PAL/HTL, temperature, series resistance and shunt resistance of $CH_3NH_3SnI_3$, $CH_3NH_3SnBr_3$ and $CH_3NH_3GeI_3$ based PSC devices. At the PAL width of 500nm, defect density of $1\times10^{14}cm^{-3}$, parasitic shunt resistance of 10^3 Ω-cm^2, series resistance of 1 Ω-cm^2 and at operating temperature 300K under AM 1.5 sun illumination, the optimum results for all three perovskite solar cell devices have been obtained which is summarized in Table 3.

4.2 Impact of variations of PAL defect density on PSC parameters

Defect density has a decisive stake in the performance of PSCs. At a PAL thickness of 500nm, the defect density of PAL of all three PSCs has been increased from $1\times10^{12}cm^{-3}$ to $1\times10^{16}cm^{-3}$, PSC parameters V_{OC}, J_{SC}, FF and PCE is investigated for it, Fig. 4(a-d). For defect density $>1\times10^{12}cm^{-3}$,V_{OC} is decreases continuously with enhancement of defect density of PAL. J_{SC} remains constant with an increase in defect density of PAL up to $1\times10^{12}cm^{-3}$ after that it decreases significantly. FF is also nearly constant up to defect density of 1×10^{14} cm^{-3} after that it drastically decreases with increase in defect density. PCE which is a function of all three-discussed parameter is decrease continuously with increase in defect density and reaches minimum value $1\times10^{17}cm^{-3}$.

4.3 Effect of simultaneous variations due to Defect density and width of PAL in PSC parameters

The contour graph of solar cell characteristics as a joint function of defect density and width of PAL for $CH_3NH_3SnI_3$ is shown in Fig. 5. Contour of FF drawn

Table 3 — Improvement of PCE over earlier simulated and experimental work.

Device Structure	V_{oc} (V)	J_{sc} (mA/cm^2)	FF(%)	PCE(%)	References
ITO/ZnO/MAGeI3/Spiro-OMeTAD/Au	1.74	16.27	64.51	18.3	[37]
FTO/TiO2/CH3NH3SnBr3/NiO	0.8	31.88	84.89	21.66	[38]
FTO/CeOx/MASnI3/Spiro-OMeTAD/Au	0.92	30.79	62.86	17.77	[35]
FTO/SnO2/(CH3NH3SnI3)/CuInSe2/Ag	0.664	45.5	62.5	18.89	[39]
ITO/ZnO/$CH_3NH_3SnI_3$/Spiro-OMeTAD/Au	1.06	31.67	77.24	25.95	This Work
ITO/ZnO/$CH_3NH_3SnBr_3$/Spiro-OMeTAD/Au	1.02	32.41	75.68	25.01	This Work
ITO/ZnO/$CH_3NH_3GeI_3$/Spiro-OMeTAD/Au	1.81	14.29	75.95	19.66	This Work

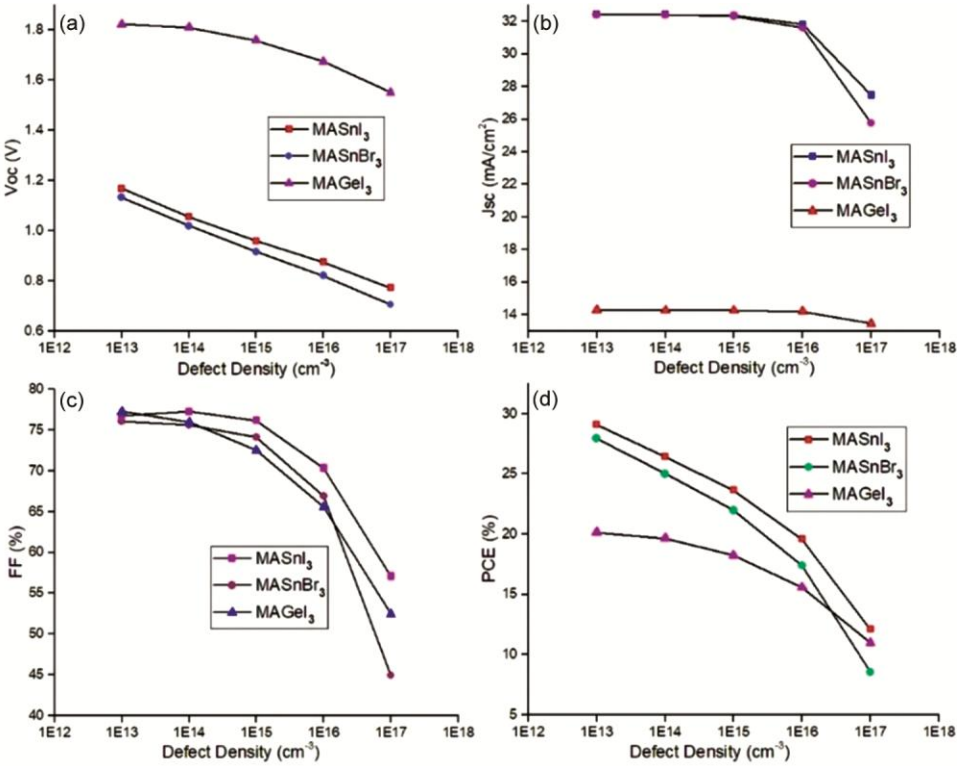

Fig.4 — Variation of (a) V_{OC}(b) J_{SC} (c) FF and (d) PCE with defect density of $CH_3NH_3SnI_3$, $CH_3NH_3SnBr_3$ and $CH_3NH_3GeI_3$.

with respect to joint function of defect density and width of $CH_3NH_3SnI_3$. It is depicted from the contour that when defect density as well as thickness are varied from $10^{10}cm^{-3}$ to$10^{17}cm^{-3}$ and 200nm to 900nm respectively, the photovoltaic parameters of perovskite material vary. There is a decrease of 23.02% in FF when thickness is above 500nm and defect density is increased from $10^{10}cm^{-3}$ to $10^{17}cm^{-3}$, V_{OC} decreased from 1.44V to 0.77V,J_{SC} decreased by 25.56% and PCE decreased from 37.25% to 11.84%. The contour graph of solar cell characteristics for defect density and width of PAL for $CH_3NH_3SnBr_3$ is shown in Fig. 6. The contour of FF is drawn as a joint function of the defect density and width of

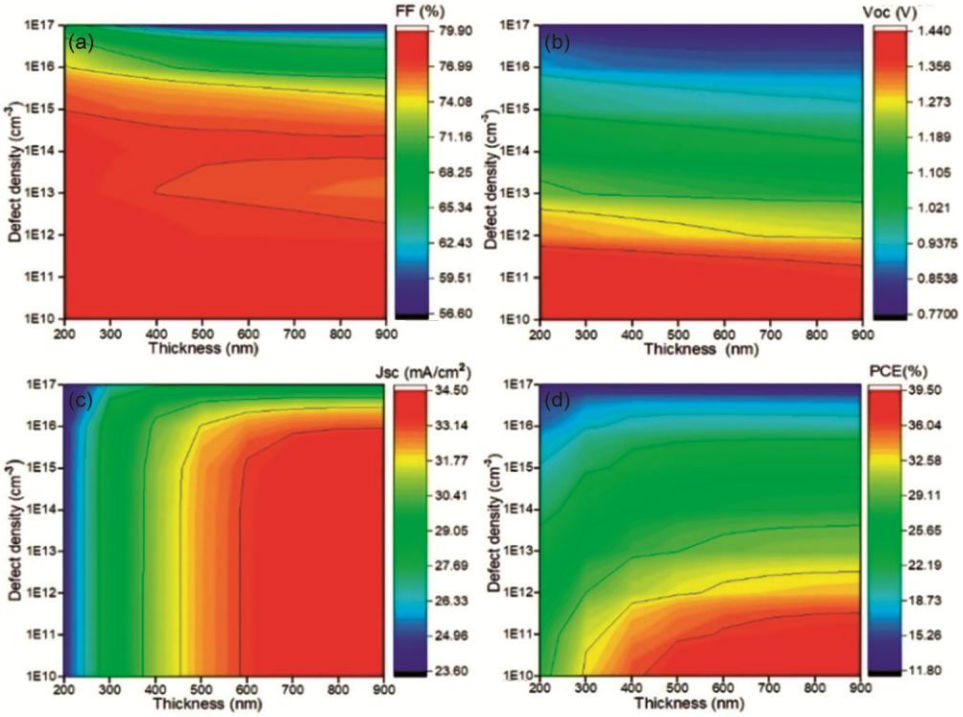

Fig. 5 — Contour graph of (a) FF (b) V_{OC} (c) J_{SC} and (d) PCE with variation of width of $CH_3NH_3SnI_3$ at different defect density.

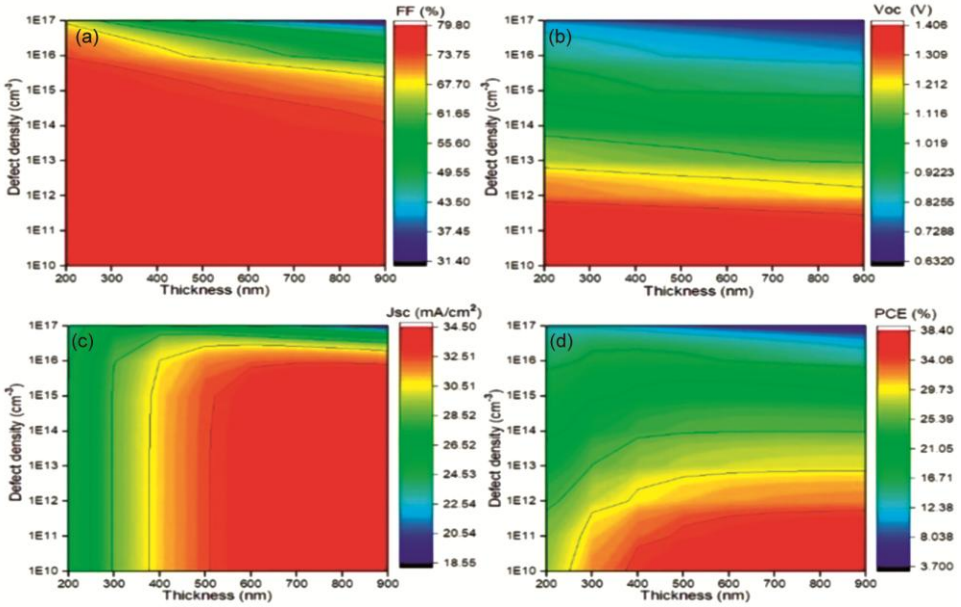

Fig. 6 — Contour graph of (a) FF (b) V_{OC} (c) J_{SC} and (d) PCE with variation of width of $CH_3NH_3SnBr_3$ at different defect density.

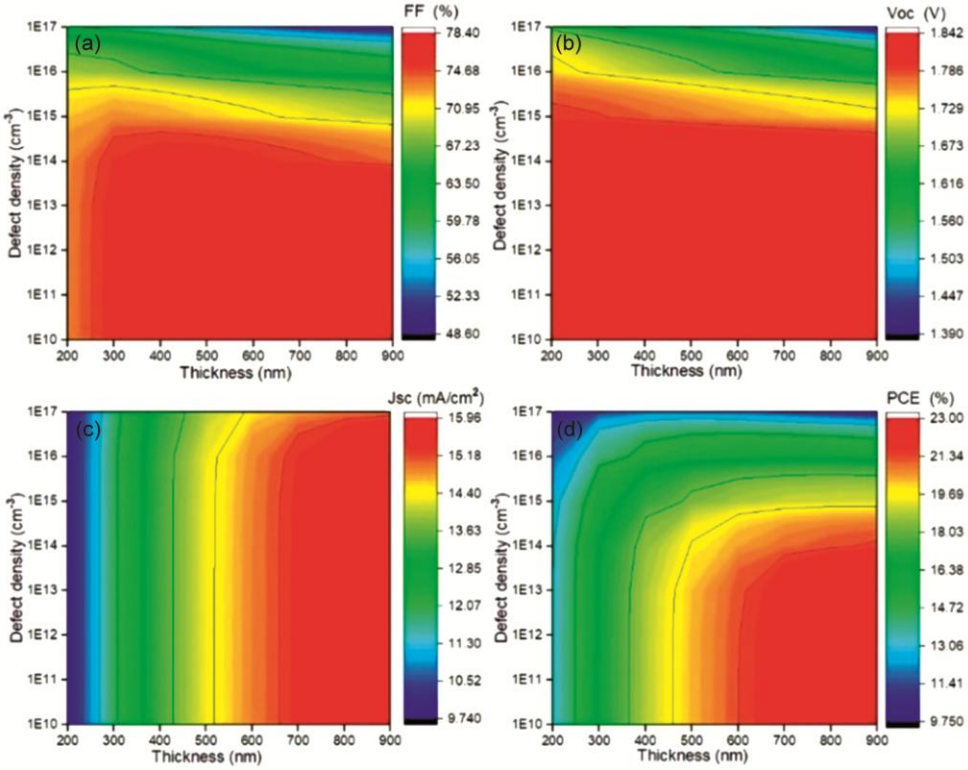

Fig. 7 — Contour graph of (a) FF (b) V_{OC} (c) J_{SC} and (d) PCE with variation of width of $CH_3NH_3GeI_3$ at different defect density.

$CH_3NH_3SnBr_3$. It is depicted from the contour that when defect density as well as thickness are varied $10^{10}cm^{-3}$ to$10^{17}cm^{-3}$ and 200nm to 900nmrespectively, the photovoltaic parameters of perovskite material vary. There is a decrease of 48.1% in FF when thickness is above 500 nm, defect density increased from $10^{10}cm^{-3}$ to$10^{17}cm^{-3}$, V_{OC} decreased from 1.406V to 0.633V, J_{SC} decreased by 42.72%, and PCE is seen to be decreased from 36.28% to 3.70%. The contour graph of solar cell characteristics for the joint function of defect density and width of PAL for $CH_3NH_3GeI_3$ shown in Fig. 7. The contour of FF is drawn as a joint function of the defect density and width of $CH_3NH_3GeI_3$. It is depicted from the contour that when defect density as well as width are increased from $10^{10}cm^{-3}$ to$10^{17}cm^{-3}$ and 200nm to 900nm respectively, the photovoltaic parameters of perovskite material vary. There is a decrease of 28.76% in FF when thickness is above 500nm and defect density is increased from $10^{10}cm^{-3}$ to$10^{17}cm^{-3}$, V_{OC} decreased from 1.812V to 1.391V, J_{SC} decreased by 31.76% and PCE is seen to be decreased from 20.31% to 10.17%. From the above studies, it can be inferred that defect density has caused a tremendous reduction in the performance of devices. The performance of $CH_3NH_3SnBr_3$ based devices has been severely degraded in comparison to $CH_3NH_3SnI_3$ and $CH_3NH_3GeI_3$. $CH_3NH_3GeI_3$ based devices have shown more stability in comparison to Sn-based devices, with an increase in defect density.

4.4 Effect of variations of layer interface defect density between ETL/PAL and PAL/HTL on the PCE

Effect of interface defect density between ETL/PAL and PAL/HTL on the on the PCE is investigated for all the three devices and shown in Fig. 8. When interface defect density between ETL/ perovskite is increased from $10^{10}cm^{-2}$ to $10^{18}cm^{-2}$ at the defect energy level of 0.6 eV, the PCE of $CH_3NH_3SnI_3$is decreased from 26.44% to 24.40% ,the PCE of $CH_3NH_3SnBr_3$ is decreased from 25.01% to 22.81% and the PCE of $CH_3NH_3GeI_3$ is decreased from 19.66% to 12.56% whereas variation of the interface layer defect density between perovskite/HTL from $10^{10}cm^{-2}$ to $10^{18}cm^{-2}$ caused PCE of $CH_3NH_3SnI_3$to reduce from 26.44% to 24.66% ,the PCE of $CH_3NH_3SnBr_3$ to reduce from 25.01% to 23.86% and the PCE of $CH_3NH_3GeI_3$ to reduce from 19.66% to 15.44%. From above result, it can be inferred that increase in interface defect density Causes significant reduction in the PCE for all three devices.

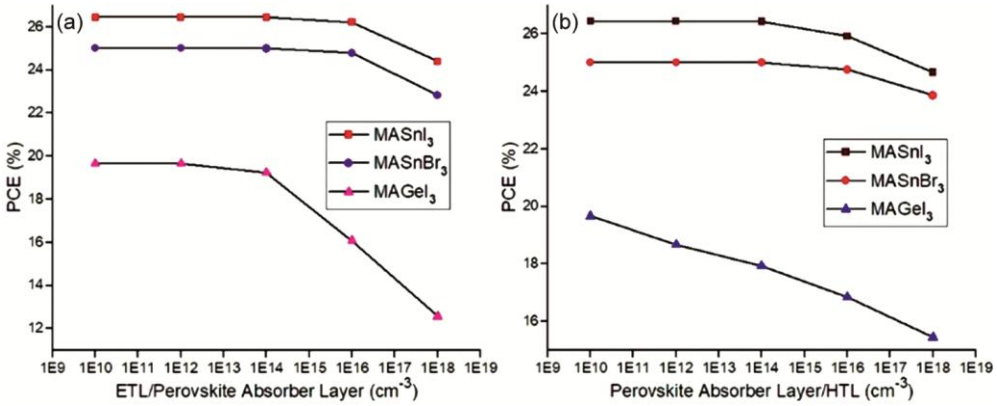

Fig. 8 — Variation of PCE with interface defect density (a) ETL/PAL (b) PAL/HTL.

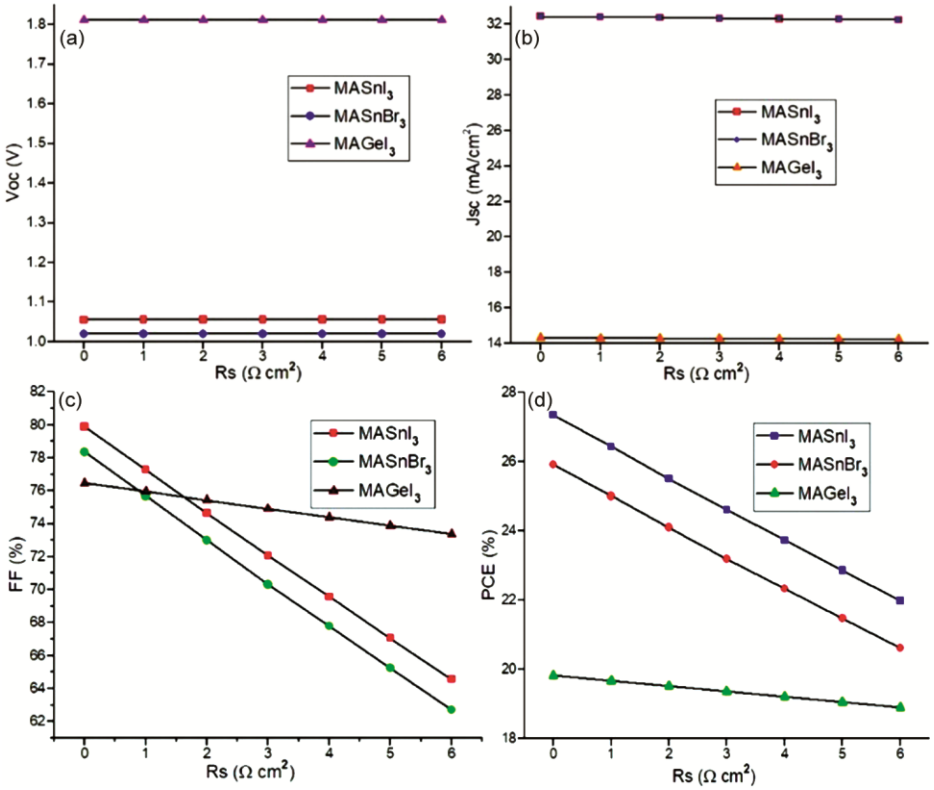

Fig. 9 — Variation in (a) V_{OC} (b) J_{SC} (c) FF and (d) PCE with respect to series resistance in $CH_3NH_3SnI_3$, $CH_3NH_3SnBr_3$ and $CH_3NH_3GeI_3$ keeping shunt resistance at 10^3 (Ω-cm^2).

4.5 Effect of variations of series resistance (R_s), shunt resistance (R_{sh}) and Temperature on PSC parameters

Figure 9 shows variation of solar cell parameter with series resistance, a very high value shunt resistance and low value of series resistance is required for high value of J_{SC} and PCE. Series resistance has direct effect on fill factor (FF) and short circuit current. Here the R_s is varied from 0-6 Ω-cm^2 with the value of R_{sh} fixed at 10^3 Ω-cm^2.V_{OC} and J_{SC} remain constant whereas FF and PCE both are reduced linearly with the increase in series resistance.This indicates that for the examined device configurations, R_S variation has no effect on the J_{SC} and V_{OC} parameters. Rate of decrease in FF and PCE is more for $CH_3NH_3SnI_3$ and $CH_3NH_3SnBr_3$ than $CH_3NH_3GeI_3$. Fig. 10 shows the variation ofsolar cell characteristics with the increase in shunt resistance. All parameters show improvement with increase in shunt resistance. R_{sh} is varied from 10^1-10^7 Ω-cm^2 with the value of R_s fixed at 1 Ω-cm^2. For the value of R_{sh}<1E+04 all the parameters V_{OC}, J_{SC}, FF

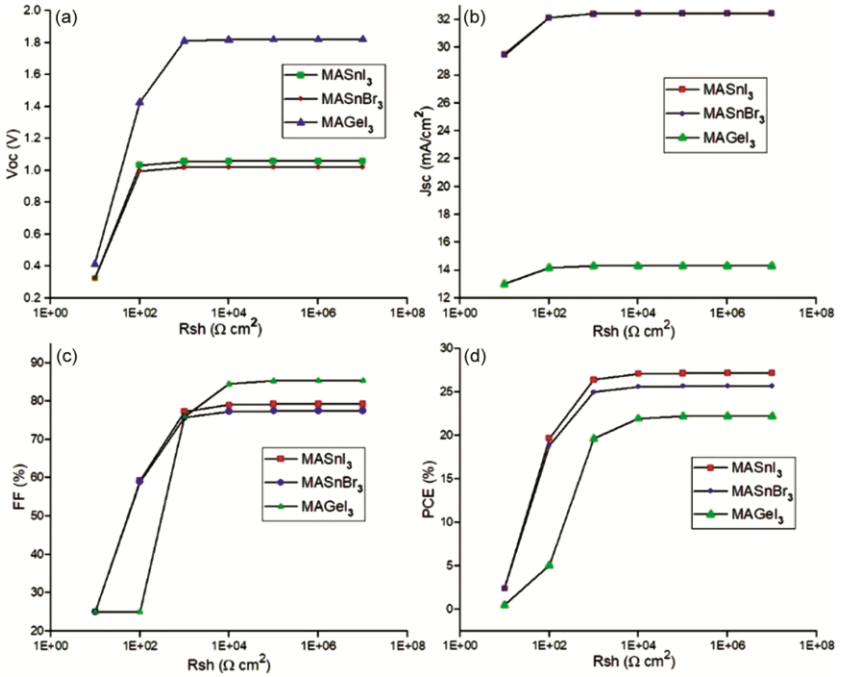

Fig. 10 — Variation in (a) V_{OC} (b) J_{SC} (c) FF and (d) PCE with respect to shunt resistance in $CH_3NH_3SnI_3$, $CH_3NH_3SnBr_3$ and $CH_3NH_3GeI_3$ keeping series resistance at 1 Ω-cm^2.

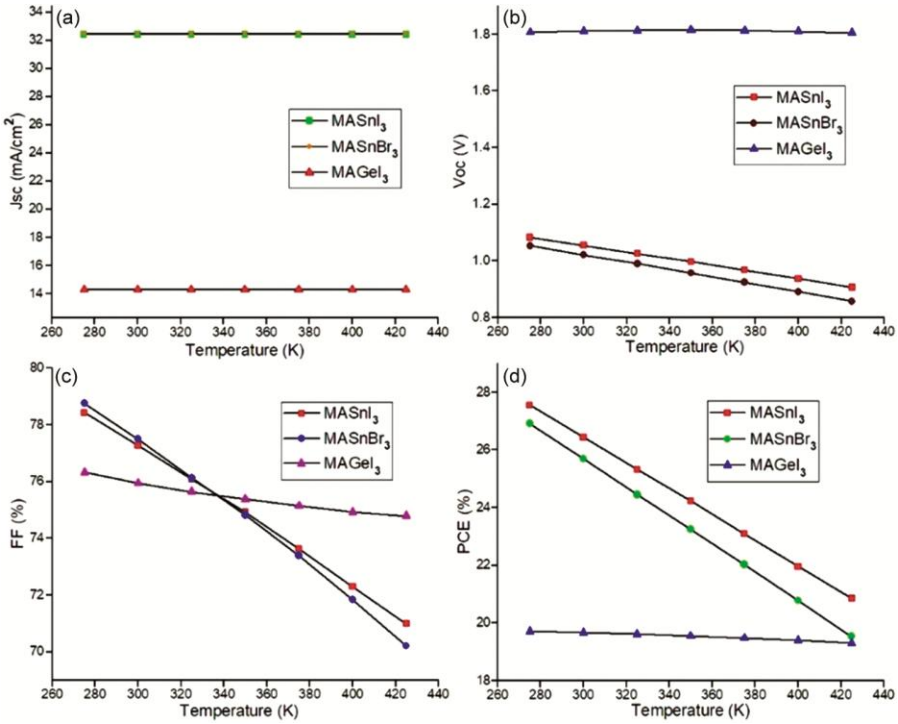

Fig. 11 — Variation in(a) V_{OC} (b) J_{SC} (c) FF and (d) PCE with respect to temperature in $CH_3NH_3SnI_3$, $CH_3NH_3SnBr_3$ and $CH_3NH_3GeI_3$.

and PCE increase with the increase in the value of shunt resistance. For the value of R_{sh}>1E+04 all parameter V_{OC}, J_{SC}, FF and PCE remain constant. Fig. 11 shows variation in solar cell parameters with respect to temperature in $CH_3NH_3SnI_3$, $CH_3NH_3SnBr_3$ and $CH_3NH_3GeI_3$. Increase in temperature causes increase in ions vibration that obstruct free flow of temperature through the carriers and has adverse effect on FF and PCE. $CH_3NH_3GeI_3$ is more stable in comparison to Sn-

based perovskite solar cell with respect to increase in temperature.

5 Conclusion

An extensive investigation of Sn and Ge-based lead-free devices has been carried out to develop stable lead-free PSCs with high efficiency. Three different lead-free devices have been modelled and their parameters have been studied. The modelled solar cells are ITO/ZnO/$CH_3NH_3SnI_3$/Spiro-OMeTAD/Au, ITO/ZnO/$CH_3NH_3SnBr_3$/Spiro-OMeTAD/Au and ITO/ZnO/$CH_3NH_3GeI_3$/Spiro-OMeTAD/Au. The solar cell parameters *i.e.* V_{OC}, J_{SC}, FF and PCE have been analyzed for different design parameters like thickness and defect density of PAL to optimize solar cell parameters. Modelling and simulation of all three devices are achieved through SCAPS-1D software, and comparative analysis of the performance of all the solar cells is studied. The effect of series and shunt resistances, interface defect density and temperature has also been studied for all three devices. Sn-based devices were found to be more efficient than Ge-based devices, but in terms of stability, Ge-based devices give superior results. The proposed devices at the width of $500\,\text{nm}$ and defect density of $1\times10^{14}\,\text{cm}^{-3}$ of PAL provide best possible results. ITO/ZnO/$CH_3NH_3SnI_3$/Spiro-OMeTAD/Au provided PCE value of 25.95%, V_{OC} of 1.06V, J_{SC} of 31.67mA/cm^2 and FF of 77.24%, ITO/ZnO/$CH_3NH_3SnBr_3$/Spiro-OMeTAD/Au provided PCE 25.01%, V_{OC} 1.02V, J_{SC} 32.41mA/cm^2 and FF 75.68% and ITO/ZnO/$CH_3NH_3GeI_3$/Spiro-OMeTAD/Au provided PCE 19.66%, V_{OC} 1.81V, J_{SC} 14.29mA/cm^2 and FF 75.95%. Sn-based devices provided very high efficiency mainly due to small band gap of perovskite material that enables increased absorption of solar energy leads to increased charge carrier generation. It has also been found that defect density of PAL has tremendous effect on PCE. The PCE obtained in the present work is compared with earlier work. The modelled devices show superior parameters than earlier work and will further contribute towards the fabrication of environment friendly lead-free device PSCs with high efficiency and stability.

References

1 Singh K A S, Mohammed M K & Shalan A E, *Sol Energy*, 223 (2021) 193.
2 Sharif R, Khalid A, Ahmad S W, Rehman A, Qutab H G, Akhtar H H, Khalid M, Afzalc S & Saleem F, *Nanoscale Adv*, 5 (2023) 3803.
3 Kojima A, Teshima K, Shirai Y & Miyasaka T, *Amer Chem Soc*, 131 (2009) 6050.
4 Green M A, Ho-Baillie A & Snaith Henry J, *Nature Photon*, 8 (2014) 506.
5 Kim G, Min H , Lee K S, Lee D Y, Yoon S M & Seok S I , *Science*, 370 (2020) 108.
6 Jiang Q, Zhao Y, Zhang X , Yang X , Chen Y , Chu Z , Ye Q, Li X , Z Yin & You J, *Nat Photon*, 13 (2019) 460.
7 Yang W S, Park B W, Jung E H, Jeon N J, Kim Y C, Lee D U, Shin S S, Seo Ja, Kim E K, Noh J H & Seok S I, Science, 356 (2017) 1376.
8 Miyata A, Mitioglu A, Plochocka P, Portugall O, Wang J T W, Stranks S D, Snaith H J & Nicholas R J, *Nat Phys*, 11 (2015) 582.
9 Chen B, Yang M, Priya S & Zhu K, *J Phys Chem Lett*, 7 (2016) 905.
10 Abate A, *Joule*, 1 (2017) 659.
11 Stoumpos C C, Malliakas C D & Kanatzidis M G, *Inorg Chem*, 52 (2013) 9019.
12 Liu X, Yang Z, Chueh C C, Rajagopal A, Williams S T, Sun Y & Jen A, *J Mater Chem A*, 4 (2016) 17939.
13 Kayesh M E, Matsuishi K, Kaneko R, Kazaoui S, Lee J J, Noda T & Islam A J A E L, *ACS Energy Lett*, 4 (2018) 278.
14 Noel N K, Stranks S D, Abate A, Wehrenfennig C, Guarnera S, Haghighirad A A, Sadhanala A, Eperon G E, Pathak S K, Johnston M B, Petrozza A, Herz L M & Snaith H J, *Energy Environ Sci*, 7 (2014) 3061.
15 Kumar R, G Kim, Karupannan H J & Prabakar S K, *J Phys Chem C*, 121 (2017) 16447.
16 Liu L Y, Zhou H, Yang W, Shang D, Shi Y, Li Z, Jiang B, Zhang X, Quan L, *et al*., *J Am Chem Soc*, 139 (2017) 6693.
17 Marshall K P, Walker M, Walton R I & Hatton R A, *Nat Energy*, 1 (2016) 16178.
18 Correa-Baena J P, Abate A, Saliba M, Tress W, Jacobsson T J, Grätzel M & Hagfeldt A, *Energy Environ Sci*, 10 (2017) 710.
19 Ono L K, Juarez-Perez E J & Qi Y, *ACS Appl Mater Interfaces*, 9 (2017) 30197.
20 Liu X, Yang Z, Chueh C C, Rajagopal A, Williams S T, Sun Y & Jen A K Y, *J Mater Chem A*, 4 (2016) 17939.
21 Ju M G, Dai J, Ma L & Zeng X C, *J Am Chem Soc*, 139 (2017) 8038.
22 Sun P P, Li Q S, Yang L N & Li Z S, *Nanoscale*, 8 (2016) 1503.
23 Ansari M I H, Qurashi A & Nazeeruddin M K, *J Photochem Photobiol C Photochem Rev*, 35 (2018) 1.
24 Stoumpos C C, Frazer L, Clark D J, Kim Y S, Rhim S H, Freeman A J, Ketterson J B, Jang J I & Kanatzidis M G, *J Am Chem Soc*, 137 (2015) 6804.
25 Gao P, Bin M Y A R & Nazeeruddin M K, *Nat Commun*, 9 (2018) 5028.
26 Krishnamoorthy T, Ding H, Yan C, Leong W L, Baikie T, Zhang Z, Sherburne M, Li S, Asta M, Mathews N, *et al.*, *J Mater Chem A*, 3 (2015) 23829.
27 De R R, Zanuccoli M, Magnone P, Sangiorgi E & Fiegna C, *Open issues for the numerical simulation of silicon solar cells*, In: Ulis 2011 Ultimate Integration on Silicon, Cork, (2011) 1.
28 Liu S, Biju V P, Qi Y, Chen W & Liu Z, *NPG Asia Mater*, 15 (2023) 1.
29 Ma F, Zhao Y, Qu Z & You J, *Acc Mater Res*, 4 (2023) 716.

30 Chen Y, Zhang M, Li F & Yang Z, *Coatings*, 13 (2023) 644.
31 Li Y, Li H, Zhong C, Sini G & Brédas J L, *NPJ Flex Electron*, 1 (2017) 2.
32 Husainat A, *et al*., *Am J Opt Photon*, (2019).
33 Hossain M K, Rubel M H K, Toki G F I, Alam I, Rahman Md F & Bencherif H, *ACS Omega*, 7 (2022) 43210.
34 Hossain A, Hasan M M, Rahman M D S & Hossain M A M, Fully Lead-Free All Perovskite Tandem Solar Cell with Improved Efficiency: Device Simulation Using SCAPS-1D, *IEEE Region 10 Symp*, TENSYMP, (2020)
35 Al-Mousoi A K, Mohammed M K A, Pandey R, Madan J, Dastan D, Ravi G, Sakthivele P & Babu G A, *RSC Adv*, 12 (2022) 32365.
36 Islam Md S, Sobayel K, Al-Kahtani A, Islam M A, Muhammad G, Amin N, Shahiduzzaman Md & Akhtaruzzaman Md, *Nanomaterials*, 11 (2021) 1218.
37 Bhattarai S & Das T D, *Sol Energy*, 217 (2021) 200.
38 Islam Md S, Sobayel K, Al-Kahtani A, Islam M A, Muhammad G, Amin N, Shahiduzzaman Md & Akhtaruzzaman Md, *Nanomaterials*, 11 (2021) 1218.
39 Gagandeep, Singh M, Kumar R & Singh V, *Optik*, 246 (2021) 167839.